

On the pinch-off of a pendant drop of viscous fluid

Diane M. Henderson,^{a)} William G. Pritchard, and Linda B. Smolka
William G. Pritchard Fluid Mechanics Laboratory, Department of Mathematics, Pennsylvania State University, University Park, Pennsylvania 16802

(Received 28 October 1996; accepted 8 July 1997)

The pinch-off of a drop of viscous fluid is observed using high-speed digital imaging. The behavior seen by previous authors is observed here; namely, the filament that attaches the drop to the orifice evolves into a primary thread attached to a much thinner, secondary thread by a slight bulge. Here, we observe that the lengths of the primary and secondary threads are reproducible among experiments to within 3% and 10%. The secondary thread becomes unstable as evidenced by wave-like disturbances. The actual pinch-off does not occur at the point of attachment between the secondary thread and the drop. Instead, it occurs between the disturbances on the secondary thread. After the initial pinch-off, additional breaks occur between the disturbances, resulting in several secondary satellite drops with a broad distribution of sizes. The pinch-off of the thread at the orifice is similar to that at the drop with one main difference: there is no distinct secondary thread. Instead, the primary thread necks down monotonically until wave-like disturbances form, resulting in pinch-off at multiple sites in between. The speed of the tips of the retreating, secondary threads after pinch-off are reported and discussed in the context of various scaling laws. © 1997 American Institute of Physics. [S1070-6631(97)02311-8]

I. INTRODUCTION

Here we present images of the pinch-off of pendant drops of viscous fluids that fall from an orifice under the action of gravity. The thread connecting the drop to the orifice necks down into thinner regions at the orifice and at the drop. The necking near the drop results in a distinct secondary thread that is separated from the primary thread by a nonmonotonic transition region, as observed by Shi, Brenner, and Nagel¹ (SBN), who previously investigated drops, and by Kowalewski,² who investigated jets. We observe (i) the lengths of the primary and secondary threads are repeatable to within 3% and 10%, respectively. (ii) A wave-like instability forms on the secondary thread. Kowalewski² observed this type of behavior in the fine-scale structure of jet breakup. (iii) Pinch-off occurs between waves on the secondary thread, rather than at the drop. (iv) After the initial pinch-off, several additional breaks occur along the secondary thread between the disturbances. The numerous breaks in the secondary thread then result in a number of secondary, satellite drops, which have a broad distribution of sizes. Their length scales are roughly 1/100th that of the drop's. This fine-scale mechanism for creating satellite drops was observed in the breakup of jets by Kowalewski.² (v) The primary thread does not evolve into a distinct secondary thread at the orifice, in contrast to results of previous experiments. Instead, it necks down monotonically, develops disturbances, and pinches-off at multiple sites between the disturbances. The separated primary thread then rapidly retreats downward from the orifice, forming the primary satellite drop, which has a length scale roughly 1/10th that of the drop's. We also present measurements of tip speeds of the retreating secondary threads after pinch-off and discuss the results in the con-

text of Eggers³ theory and other scaling laws. The tips retreat with a power-law dependence on the time away from the pinch-off time. The power is dependent on the shape and length of the retreating thread.

The pinch-off of a viscous drop of fluid has been widely investigated. See, e.g., studies of pendant drops in water by Edgerton *et al.*⁴ and Peregrine *et al.*⁵ The results of the latter were well-modeled by Schulkes,⁶ who numerically integrated a potential flow formulation of Euler's equations for the pendant drop. SBN¹ presented photographs of the pendant drop using fluids with a large range of viscosities. They showed that the primary thread evolved into a secondary thread and even into a tertiary thread in experiments using fluids with a similar viscosity as those used here, but a much larger orifice. Their numerical computations using the approximate Navier–Stokes model developed by Eggers and Dupont⁷ also showed the development of the secondary threads. When a noise source was explicitly introduced, the model showed the development of a cascade of threads with decreasing sizes, each of which was well-described by the similarity solution of Eggers.⁸ SBN¹ also showed a photograph in which a thread of 200 cP oil exhibited an instability, characterized by localized “blobs” rather than the waves observed herein. Brenner *et al.*⁹ explained the disturbances as an instability of Eggers⁸ similarity solution. Zhang and Basaran¹⁰ (ZB) conducted a comprehensive study of how the drop's evolution varied as a function of flow rate, viscosity, surface tension, thickness of the tube wall, and radii of the orifice.

The study of the pendant drop is closely related to that of jet stability [see Boggy¹¹ and Bechtel *et al.*¹² (BCF) for reviews]. In particular, in the pendant drop experiment, we may consider the primary and secondary threads as viscous jets; the primary thread does not exhibit a classical wave-like instability that leads to breakup. Instead, it becomes unstable to the secondary thread, which does exhibit a wave-like in-

^{a)}Corresponding author: Phone: 814-863-0516, Fax: 814-865-3735; Electronic mail: dmh@math.psu.edu

stability that leads to breakup. According to Rayleigh's¹³ classical result, a constant flow, inviscid, azimuthally uniform jet is unstable to perturbations with wavelengths larger than πD , where D is the diameter of the jet; the most unstable wavelength is about $1.43\pi D$. The experiments on jets by Donnelly and Glaberson¹⁴ showed that there was no preferred unstable wavelength unless the jet was perturbed with a particular periodicity. In the presence of such perturbations, the growth rates of the unstable wavelengths agreed well with Rayleigh's¹³ calculations; growth rates of instabilities on glycerin and water jets agreed reasonably well with the calculations of Chandrasekhar¹⁵, who included viscosity in his linear calculation of stability. Donnelly and Glaberson¹⁴ noted that the axial dependence of the instabilities was not sinusoidal, a result probably due to nonlinearity. Goedde and Yuen¹⁶ addressed this aspect of the problem by measuring separately the growth rates of the swells and the necks. Individually each did not grow with a constant exponential growth rate, but the difference between the two did grow at a constant exponential rate that agreed with the prediction of Chandrasekhar.¹⁵ BCF expanded the Navier–Stokes equations with respect to a small slenderness ratio of thread width to length. Their model is different from Eggers and Dupont's⁷ in that the expansion is self-consistent. BCF¹² showed that a jet is linearly unstable at leading order to perturbations with no preferred length scale or high-wavenumber cutoff. However, the inclusion of higher-order terms recovers a Rayleigh-type cutoff for the unstable wavelengths. Thus, BCF conjecture that as the slenderness ratio of the jet approaches zero, the jet will become unstable to perturbations of all wavelengths, and none will be selectively amplified.

Kowalewski² also observed instabilities of viscous fluid jets when they were perturbed with high-frequency disturbances. Rather than focusing on the wavelengths for instability, he was particularly concerned with the details of the jet breakup. He observed behavior very similar to that described herein for *drops*, when using fluids with viscosities ranging from about 11 to 320 mm²/s. The length of the secondary threads that he observed varied from about 20 μ m to several millimeters as a function of fluid parameters. Further, he observed the formation of distinct secondary threads, their instabilities to disturbances with a broad distribution of length scales, and multiple pinch-offs resulting in several secondary satellites of various sizes when the fluid viscosities were 46 mm²/s and larger.

Drop deformations and the formation of satellite drops have also been widely investigated in other liquid bridge systems. See Stone¹⁷ for a review of drop deformations due to motions in a viscous, ambient fluid. Stone, *et al.*¹⁸ conducted experiments investigating the end-pinch and capillary wave instabilities of extended threads of viscous fluids during contraction. Stone and Leal¹⁹ used a boundary-integral method to model these experiments. The dynamics of the instability, both in experiments and numerics, depended on the ratio of thread fluid to ambient fluid viscosities. Lafrance²⁰ looked at satellite formation due to the breakup of a jet with an imposed perturbation. His measurements of growth rates and radii of main and satellite drops

were well-modeled by the boundary-integral formulation for inviscid jets employed by Mansour and Lundgren.²¹ Tjahjadi, *et al.*²² looked at the breakup of a fluid filament in an external fluid; the filament was formed by a shearing action in a Couette device. They observed the formation of as many as 19 satellite drops and noted that the number of satellites and their size distributions, which varied over three orders of magnitude, also depended primarily on the ratio of the viscosities of the filament fluid to ambient fluid. Their experimental results were well-captured by their computations of Stokes equations. Papageorgiou²³ also presented a Stokes model of jet breakup and satellite formation. The instability of coating films around vertical fibers may result in drop formation when the film thickness is larger than some critical value; see, e.g., Kalliadasis and Chang,²⁴ who obtained a prediction for the critical thickness of the film. Experiments on the collapse of a soap-film bridge by Cryer and Steen²⁵ are also similar to results herein; the soap film stretched between two open endrings. Upon separation of the endrings, the film collapsed by necking at the midsection, forming a thin filament that broke up into a primary and several secondary satellite drops.

Here, in the pendant drop experiment, the secondary satellites result from the pinch-off between wave-like disturbances along the secondary thread. In any one experiment, the disturbances do not exhibit a particular periodicity, and an approximate periodicity varies among experiments. The resulting, secondary satellite drops have a fairly broad distribution of sizes. These observations are consistent with BCF's¹² conjecture that as the slenderness ratio approaches zero, the wavelengths of instability of the jet will not have a preferred wavelength. They are also consistent with Kowalewski's² observations of jet breakup. We further observe, however, that the sizes of the disturbances and, correspondingly, the sizes of the secondary satellite drops, are consistent with a Rayleigh-type, wavelength cutoff. The higher-order terms in the BCF¹² model are required to capture this cutoff.

Eggers³ conducted an investigation of the development of the thread both before and after pinch-off by calculating the asymptotic solutions of the Navier–Stokes equations through the pinch-off point. He provides a prediction of the speeds of the retreating threads after pinch-off in terms of the similarity variable $\xi = z'/t'^{1/2}$, where $z' = (z - z_0)/l_\nu$ and $t' = (t - t_0)/t_\nu$ are nondimensional measures of the distances and times from the location of pinch-off, z_0 , at time, t_0 . The viscous length and time scales are $l_\nu = \rho \nu^2 / \gamma$ and $t_\nu = \rho^2 \nu^3 / \gamma^2$, where ν is the (kinematic) coefficient of viscosity, γ is the (dynamic) surface tension, and ρ is the density of the fluid. He predicts that the speed of the retreating neck after pinch-off is given by

$$v_{\text{neck}} = \frac{\xi_{\text{neck}}}{2} |t'|^{-1/2}, \quad (1)$$

with

$$\xi_{\text{neck}}/2 \approx 8.7 \quad (2)$$

In Sec. III C we present measurements of the speeds of the tips of retreating threads. We determine a power law for the

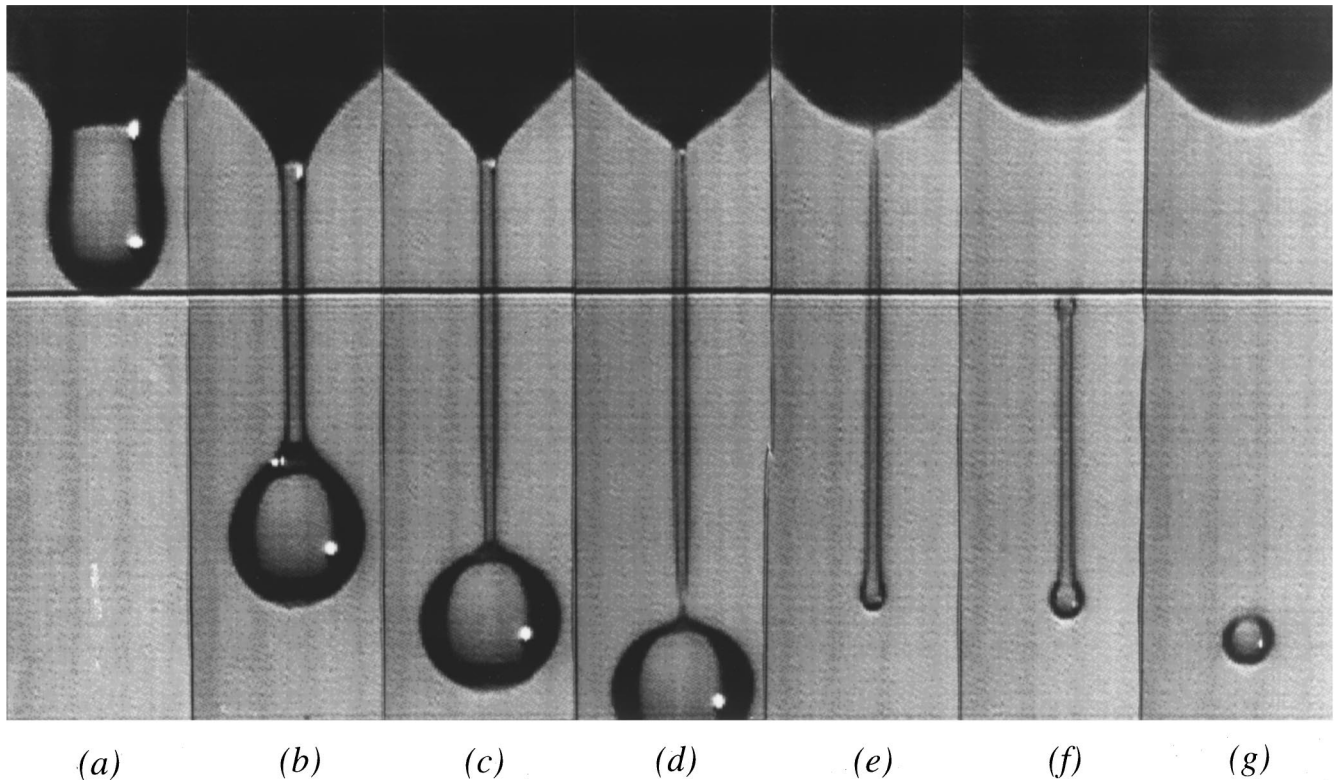


FIG. 1. Evolution of a drop from its formation through the formation of a primary satellite drop. The resolution is $93.3 \mu\text{m}/\text{pixel}$. The size of each image is $5.88 \times 22.20 \text{ mm}^2$. The relative times of each image are (a) 0 s, (b) 0.0587 s, (c) 0.0657 s, (d) 0.0703 s, (e) 0.0763 s, (f) 0.0817 s, (g) 0.0930 s; $\nu = 92 \text{ mm}^2/\text{s}$.

measured data for comparison with (1) and (2). Kowalewski² also compared the measured retraction speeds of the secondary threads of his pinched-off jets with Eggers³ theory and found the measurements to be much less than predicted.

In the remainder of the paper, we discuss the experimental apparatus (in Sec. II) and the observations (in Sec. III). A short summary of results is provided in Sec. IV.

II. EXPERIMENTAL APPARATUS

The experimental apparatus consisted of a Lucite, sinked reservoir, oils with viscosities of about $100 \text{ mm}^2/\text{s}$, a digital imaging camera and processor, and computer hardware and software for image processing.

The fluid flowed under gravity from a 32 cm^3 reservoir, which was open to the atmosphere, into a tube of length 24.7 mm, through a needle valve, which controlled the flow rate, and finally through a lower tube of length 81.5 mm with inner and outer radii of 1.41 and 1.92 mm. The 0.50-mm-wide edge of the orifice was machined flat so that the dripping oil wetted the entire surface area between inner and outer edges, but did not climb up the outside face of the tube. We found that if the orifice edge was angular, rather than flat, then the fluid climbed part-way up the side with an uneven and irreproducible contact line. In all of the experiments, except those represented in Fig. 4, the period of the drops was about 30 s/drop. The reservoir/tube/orifice apparatus was set on a hydraulic, vibration isolation table and enclosed in a Lucite box with one side made of a plastic

curtain. The box was not temperature controlled, but it isolated the drops from air currents. Imaging was done through a hole in the plastic curtain.

The oils used were a commercial vegetable oil (Fig. 1) and a silicone oil from Dow Corning Corporation (Figs. 3, 5, and 7). A Canon-Fenske viscometer in a constant temperature water bath was used to measure the oils' viscosities as a function of temperature. Linear relationships between viscosity in square millimeters per second and temperature T in degrees celsius were established for the two oils: $\nu = -3.96T + 181.49$ for the vegetable oil and $\nu = -2.02T + 149.03$ for the silicone oil. The temperature of the oil during each experiment was measured with a digital thermometer inserted into the reservoir, and the corresponding viscosity inferred from the above relationships. In Sec. III we report these measured temperatures. The temperature of the drop upon exiting from the orifice was not measured. The surface tension of the oils at room temperature was measured using a Fischer model 21 tensiometer to be 33.4 dyn/cm for the vegetable oil and 21.5 dyn/cm for the silicone oil. The measured density of the vegetable and silicone oils was 0.968 and 0.928 g/cm^3 . The ranges of the viscous length and time scales were $0.398 \text{ mm} \leq l_\nu \leq 0.453 \text{ mm}$ and $0.0016 \text{ s} \leq t_\nu \leq 0.0020 \text{ s}$.

Images and videos of the drops were obtained using a Kodak Ektapro 1012 EM Motion Analyzer comprising a high-gain digital imager, a processor, and electronic memory. The drops were illuminated from behind with a 600 W lamp that was powered during the time (about 0.16 s) that

the drop was imaged. The spatial resolution of the images is listed in the caption for each figure. The temporal resolution varied from 3000 images/s as shown in Fig. 1 to 12 000 images/s as shown in Figs. 3, 5, and 7. The desired frames were downloaded via an IEEE-488 GPIB interface to a PC. Adobe Photoshop software was used to sharpen the images. The speeds of the retreating threads were obtained by determining the leading edges of the thread in successive frames. The leading edge was defined to be a 5% increase in gray level over background values.

The measured speeds of the retreating threads are presented in Sec. III C and discussed in the context of Eggers³ predictions and other scaling laws. For this comparison, we graphed the measured velocities, normalized with respect to t_v/l_v , as a function of time (t') from pinch-off on a log-log scale. The time of pinch-off, t_0 , was determined empirically by varying it until the data correlated best to a line. Bounds for the choice of t_0 are discussed in Sec. III C. The correlation was done using a least-squares fit with MATLAB; correlation coefficients are reported in Sec. III C.

Because the shortest exposure time of the images was 1/12 000 s, some of the fine scale features of the threads that evolved on faster time scales were blurred in our images. For example, near pinch-off, the measured speeds ranged from 1000 to as much as 4000 mm/s in one experiment. Retreating threads with speeds this high were displaced several pixels in one frame; therefore, our measurements of the speeds near pinch-off could be in error by several pixels. This error affects only the few data points initially after pinch-off. After the first few data points the speeds of the retreating threads averaged about 500 mm/s and decreased to about 100 mm/s. For a speed of 450 mm/s, the threads displaced 2 pixels during one image. Measurements of the sizes of the secondary satellite drops shown in Fig. 4 were taken after the satellites had achieved the average speed; the measurements of their lengths could be in error by 2 pixels.

III. OBSERVATIONS

Here we discuss the evolution of the pendant drop in terms of its large-scale (Sec. III A) and small-scale (Sec. III B) behavior. Section III A includes discussions of the primary thread, its transition to a secondary thread at the drop, its monotonic decrease at the orifice, and its contraction from the orifice into the primary satellite drop. Section III B includes a discussion of the instability of the secondary thread, pinch-off at the drop and at the orifice, and the secondary satellite drops. In Sec. III C the velocities of the retreating tips of the secondary threads after pinch-off are presented.

A. Large-scale behavior

Figure 1 comprises images of the drop development to the time of the formation of a spherical primary satellite drop. (All of the images in Fig. 1 are from one experiment.) When the drop first appears out of the orifice, it forms a uniform cylinder of fluid with a rounded leading edge. In Fig. 1(a) this cylinder has begun to neck down so that its radius is no longer uniform. In Fig. 1(b) the pendant drop has necked down so that it now consists of a drop attached to the orifice through a primary thread that is essentially a uniform

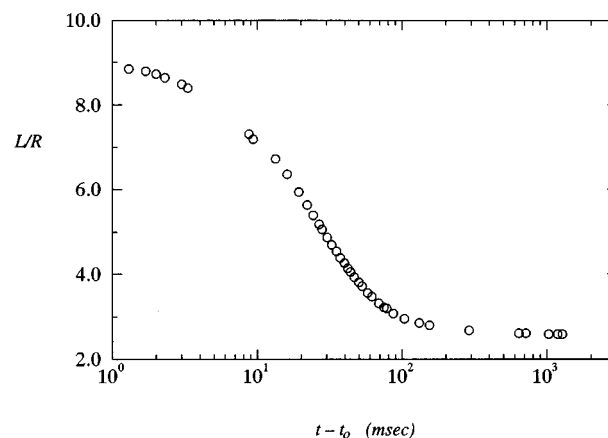


FIG. 2. Distance, L , of the leading edge of the drop, normalized by the radius of the orifice, as a function of time (in milliseconds) away from the pinch-off point. $\nu = 95.0 \text{ mm}^2/\text{s}$.

cylinder of fluid. In Fig. 1(c) the thread has lost its uniformity. It has started to neck down near the trailing edge of the drop, which is essentially spherical. In Fig. 1(d) the thread has necked down considerably at the edge of the drop. This region of rapid necking shows the nascent formation of the secondary thread observed by SBN¹ for drops and Kowalewski² for jet breakup. The time resolution in Fig. 1 does not show the further necking of the secondary thread. Figures 3(a) and 5 show a magnification of this necking region in two experiments using silicone oils with higher temporal resolution. Necks similar to the ones shown in Figs. 3(a) and 5 were also observed using the vegetable oil, but are not resolved in Fig. 1. Figure 1(d) also shows that the diameter of the thread has begun to decrease at the orifice. A rapid necking occurs at the orifice as shown in Fig. 1(e). Magnifications of this region are shown in Figs. 3(b) and 7 for experiments using silicone oils. [Again, the behavior at the orifice for the vegetable oil was like that shown in Figs. 3(b) and 7, but is not resolved in Fig. 1.] Between Figs. 1(e) and 1(f), pinch-off occurred at the orifice. The top of the primary thread then falls rapidly, while the bottom falls a slight amount. The two ends join, forming a primary satellite drop, which is shown in Fig. 1(g) after it has become spherical and has begun its downward descent.

Figure 2 shows the variation of the location of the leading edge of the drop normalized by the orifice radius as a function of time before pinch-off, t_0 , for the vegetable oil. ZB¹⁰ show similar data for experiments in which they varied the fluid viscosity, flow rate, and orifice radius. Because our parameters do not overlap theirs, a direct comparison is not possible. However, ZB also measured the limiting length of the drops (the length from the orifice to the tip of the drop just before pinch-off) as a function of flow rate (their Fig. 12) and as a function of surface tension (their Fig. 20). Table I shows the fluid properties and measurements of the ratio of limiting length to orifice radius for two of our experiments and one of ZB's. For these three experiments, the viscosities, orifice radius, and flow rates were comparable; the surface tensions varied significantly. Our results show that an increase in surface tension at a fixed viscosity caused a com-

TABLE I. Fluid properties and measurements of limiting lengths for experiments herein and for one from ZB (denoted by an asterisk). The orifice sizes and flow rates were 0.19/0.16 cm and $6 \times 10^{-3}/1 \times 10^{-2}$ ml/min for present/ZB.

Viscosity (mm ² /s)	Surface tension (g/s ²)	Limiting length radius/orifice
100	21.5	14.9
95	33.4	8.8
92*	66*	64*

parable decrease in the limiting length. This result is in marked contrast to the measurements of limiting length for an (essentially) inviscid fluid (water, and water/surfactant mixtures), for which ZB found (their Fig. 20) that an increase in surface tension caused an increase in limiting length.

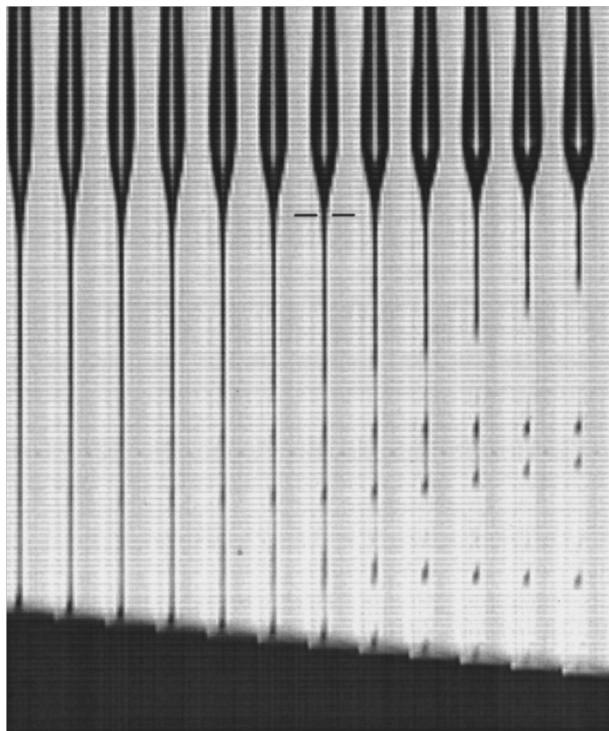
Figure 3(a) shows magnified views of the development of a secondary thread similar to the one beginning to evolve in Fig. 1(d). [All of the images in Fig. 3(a) are from one experiment.] The drop is visible at the bottom of each image, and the primary thread is visible at the top of each image. Figure 3(a-i) shows that the primary thread has necked down abruptly and is separated from the secondary thread by a slight bulge. This bulge is presumably due to the ejection of fluid from the region of large curvature. The secondary thread stretches; the bulge becomes more pronounced; then a

disturbance begins to grow on the secondary thread. The nascent disturbance is visible in Fig. 3(a-iii) and is pronounced in Fig. 3(a-vii), the frame before the first pinch-off.

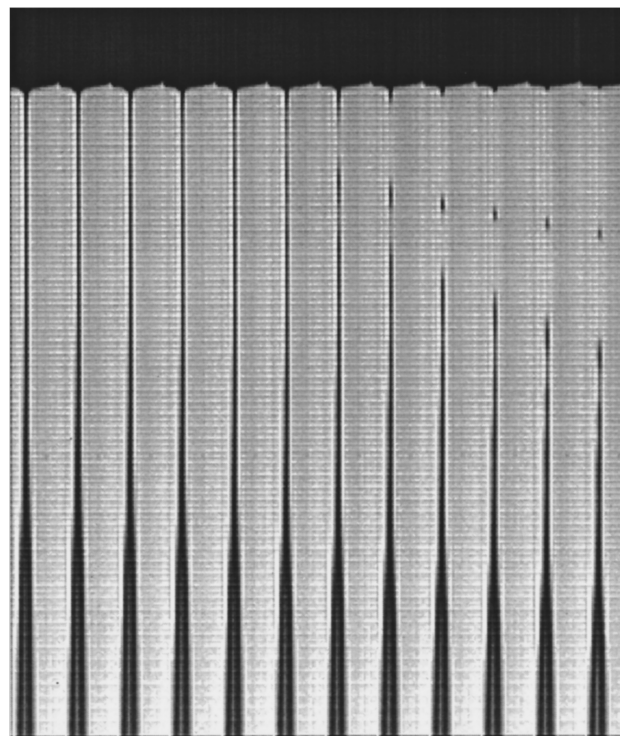
Figure 3(b) shows a magnified view of the necking of the primary thread at the orifice, similar to the behavior evident in Fig. 1(e). [All of the images in Fig. 3(b) are from one experiment.] Here the primary thread necks down and becomes unstable in a fashion similar to the behavior near the drop, except that the distinct transition from primary to secondary thread is absent at the orifice. This absence of a distinct secondary thread is in contrast to observations by SBN,¹ who did observe the formation of a distinct secondary thread, and even a tertiary thread at the orifice, as discussed in Sec. III(b). They also observed the tertiary thread at the drop. We note that we examined the behavior of the primary thread at the orifice for distances further down the thread than shown in Fig. 3(b), and saw no evidence of the curvature associated with the transition from a primary thread to a distinct secondary thread. [The resolutions of Figs. 3(a) and 3(b) are the same.]

The large-scale behavior at the drop end in which a secondary thread evolved from a primary thread occurred in every experiment. Figure 4 shows measurements of the distance from the orifice to the transition region between the two threads as a function of inverse flow rate. There is a slight trend for the distance to decrease with decreasing flow rate. The range of flow rates, where 31–134 s/drop corre-

(i) (ii) (iii) (iv) (v) (vi) (vii) (viii) (ix) (x) (xi) (xii)



(a)



(b)

FIG. 3. (a) Transition of the primary thread to secondary thread at the drop. The resolution is 28.8 $\mu\text{m}/\text{pixel}$. The size of each image is $0.46 \times 6.85 \text{ mm}^2$. The time interval between successive images is 1/12 000s. The lines in (a-vii) show the reference point for measurements shown in Fig. 4; $\nu = 106 \text{ mm}^2/\text{s}$. (b) Necking of the primary thread at the orifice to a thinner region that becomes unstable. [The resolution is the same as in (a)].

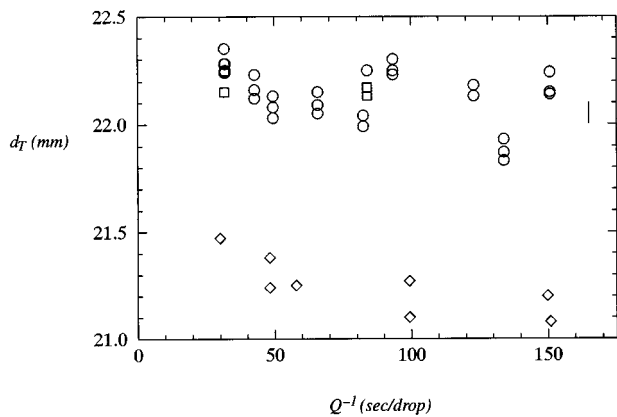


FIG. 4. Distance of the transition region measured from the orifice, d_T , to a line similar to the one shown in Fig. 3(a-vii), as a function of inverse flow rate, Q^{-1} , for various temperatures: (○) 20.9–21.4 °C, (□) 21.5 °C; (◇) 22.4–22.6 °C and corresponding viscosities (○) 106.8–105.7 mm²/s, (□) 105.5 mm²/s, (◇) 103.7–103.3 mm²/s. The vertical line at the right is the error bar.

sponded to 5.5 and 1.2×10^{-4} ml/s, was such that the experiment always involved a pendant drop, rather than a jet. The main result shown here is that the location of the transition region was reproducible to within 3% among experiments when the temperature, and correspondingly the fluid viscosity, was about constant. When the temperature was increased by about 1 °C, or about 5%, the viscosity decreased by about 2%, and the distance to the transition region decreased by about 5%. [The measurements of the distance to the transition region were taken from images like the ones in Fig. 3(a). The vertical line in Fig. 3(a-vii) shows the chosen location of the transition between primary and secondary threads. This point was chosen from the image before pinch-off, at the location where the width of the secondary thread increased an observable amount.)

The contraction of the primary thread after pinch-off from the orifice is qualitatively consistent with the numerical results of Schulkes,²⁶ who used the Navier–Stokes equations to investigate the stability of a contracting fluid filament with radius R . He showed that the occurrence of end-pinch-off, the necking behind, and the separation of the bulbous end from the filament, is dependent on the Ohnesorge number, $Oh = \nu(\rho/\gamma R)^{1/2}$. In particular, he found that if $Oh \geq O(1)$ then the fluid filament remained stable as it contracted into a spherical shape. He also noted that his numerical results did not show the growth of a Rayleigh-type instability and conjectured that such an instability was absent because the time scale for its growth was large compared to the time scale for filament contraction. In the experiments herein, $Oh = 1.3$ for the primary thread. It remained stable to the end-pinch-off instability, in agreement with Schulke's results. Further, in all but a few experiments, the primary thread was stable to a Rayleigh-type instability during contraction. For example, in Figs. 1(e)–1(g) there is no wave-like instability on the primary thread. However, in a few experiments, such a wave-like disturbance did grow on the primary thread during its contraction. This result is consistent with Schulke's conjecture concerning time scales. In the experiments, the e -folding

time for the most unstable Rayleigh mode was $\sim 10^{-3}$ s, which is about the time that passed between the primary thread's pinch-off at the orifice until its length was about equal to πD (the length of Rayleigh's cutoff instability). Since it happens here that the time available for an instability to grow is about equal to the e -folding time for growth, it is not surprising that the primary thread remained stable during most experiments, but did become unstable in a few experiments. Further, despite the presence of wave-like instabilities in a few experiments, the primary threads always contracted to form only one satellite drop for oils with viscosities of about 100 mm²/s. We note that before pinch-off, the time period during which the primary thread was long enough to exhibit a Rayleigh-type instability was about two orders of magnitude larger than the e -folding time for the growth of the most unstable Rayleigh mode. Nevertheless, instead of becoming unstable to a Rayleigh-type instability, the primary thread became unstable in a different fashion; it developed the secondary thread.

These results are consistent with previous experimental results. For example, Hauser *et al.*²⁷ did not observe the Rayleigh-type instability during the contractions of threads using glycerol with a viscosity of 881 cP. Stone *et al.*¹⁸ looked specifically at the end-pinch-off instability of a deformed thread in a quiescent, ambient, viscous fluid. If the thread was not long enough for the contraction time to admit a Rayleigh-type instability, then the end-pinch-off instability was the only one observed. If the length was long enough, then the end-pinch-off instability occurred first, but capillary waves (a Rayleigh-type instability) also evolved.

Preliminary experiments with a 200 mm²/s oil show that the primary thread does become unstable to a Rayleigh-type instability after the formation of a secondary thread at the drop, but before pinch-off at the drop. In these experiments the wave-like instabilities grew sufficiently large that the primary thread broke-up into several satellite drops during contraction. This instability does not appear to be the same as the more localized blobs that formed on the neck of a 200 cP fluid observed by SBN.¹

Brenner, *et al.*⁹ examined the stability of Eggers⁸ similarity solution to perturbations with wavelengths, λ , for which $l_v t' \ll \lambda \ll l_v t'^{1/2}$ and found that the perturbations either decayed or grew depending on the value of the similarity variable compared to its value at the stagnation point of the thread. They said that the unstable perturbations could form either *necks* or *blobs*, where a neck is the instability that we are calling the transition region between primary and secondary threads, and a blob would include the instability that we are referring to as the wave-like disturbance on the secondary thread. In comparing their calculations with our observations, we find that (1) the instability of the primary thread to secondary thread could not be explained by their mechanism, and (2) the wave-like disturbances on the secondary thread could be explained by their mechanism.

With regard to (1), the primary thread becomes unstable to the secondary thread at a time for which $t' > 1$, so that neither Eggers⁸ similarity solution or the range of possible perturbation wavelengths by Brenner *et al.*⁹ is valid. Here t' is measured with respect to the pinch-off, which occurs in

the secondary thread after the necking instability. It is not measured from a singular time that would have resulted if the primary thread had converged to Eggers' similarity solution and then pinched-off.

With regard to (2), Brenner *et al.*⁹ assumed a perturbation wavelength in the range $l_p t' \ll \lambda \ll l_p t'^{1/2}$. In the present experiments, $l_p \cong 0.4$ mm. Then, an upper bound on the disturbance wavelength obtained by taking $t' = 1$ would be about 0.4 mm. This value is about equal to the wavelength of perturbations we observe herein, which varied between about 0.4 and 0.8 mm. Further, the theory predicts that the wave-like instability should occur on that portion of the thread for which $\xi < \xi^*$, where ξ^* is the value of the similarity variable at the stagnation point in the thread. This stagnation point is close to the point of minimum thickness of the thread. This prediction is consistent with our data, in which the wave-like instability occurs on the portion of the thread near the drop.

B. Small-scale behavior

Figure 5 shows a more magnified view of a secondary thread similar to the ones evident in Fig. 1(d) and the one shown in Fig. 3(a). (All of the images in Fig. 5 are from one experiment.) The drop is falling from right to left, so that it is visible in Figs. 5(a)–5(f) at the left of each image and the primary thread is visible at the right of each image. Figures 5(a) and 5(b) show the secondary thread connecting the drop to the primary thread before instabilities develop. The transition region of large slope between the primary and secondary threads ends at 20.5 mm from the orifice. The location of the right-hand edge of Fig. 5 is 19.7 mm from the orifice.

Figure 5(c) shows the onset of the evolving instability in the secondary thread, whose slenderness ratio of width to length is about 0.005. The secondary thread pinches off first at a time between those of Figs. 5(d) and 5(e). The pinch-off point is 0.73 mm from the drop, showing that pinch-off does not actually occur at the drop. There are further pinch-offs as seen in Figs. 5(f)–5(h). These multiple pinch-offs result in several secondary satellite drops of varying sizes. Multiple pinch-offs and secondary satellite formation were also observed by Kowalewski² in secondary threads during jet break-up. Figures 5(h)–5(q) show that the speeds of the secondary satellite drops are fairly constant as they travel away from the pinch-off site, indicating that gravity is not important in describing their motions in this time period. For example, the time interval in Figs. 5(h)–5(q) is 8×10^{-4} s, during which time two drops traveled 0.8 mm upward. The effect of gravity over this time period would be to accelerate the drops downward a distance of $\sim 10^{-5}$ mm, which is negligible compared to the drop's actual motion.

The length of the secondary thread before pinch-off was reproducible to within 10%. Its variation from 3.65 to 4.05 mm occurred when the viscosity and flow rates were held constant. It also occurred when the temperature varied by about 5%, corresponding to a viscosity variation of about 2%. Further, a variation in flow rate from 31 to 134 s/drop, i.e. from 5.5 to 1.2×10^{-4} ml/s, also resulted in the same variation in secondary thread length. Thus, the reproducibility of the secondary thread length is probably dominated by the stochastic nature of the instabilities that cause thread

breakup. The small changes in viscosity and the variations in flow rates (that correspond to pinch-off of a pendant drop, rather than breakup of a jet) appear to be secondary effects.

The contraction of the secondary thread shown in Figs. 5(h)–5(m) shows that initially the secondary thread does not have a uniform cross-sectional area because the wave-like disturbances are still evolving on it. Thus, this instability will preclude the possible end-pinching instability described by Schulkes,²⁶ and we cannot compare his results to ours. Nevertheless, in the contraction of the secondary thread shown in Figs. 3(a-x)–3(a-xii), the secondary thread initially has a uniform cross sectional area and $Oh = 7.6$. In agreement with Schulkes's calculations for contracting filaments with $Oh \geq 1$ this thread does not exhibit the end-pinching instability.

The small-scale behavior described above, in which the secondary thread became unstable and resulted in pinch-off, occurred in all of the experiments. However, the details of the instability were not reproducible among experiments. Figure 6 shows a graph of the sizes of the secondary satellites formed in the secondary thread for each of six experiments. The size of the secondary satellites was determined as the area of an ellipse with major and minor axes of lengths $2a$ and $2b$ corresponding to the measured dimensions of the secondary satellites. They were normalized by the cross-sectional area of a right-circular cylinder with diameter, $D = 1$ pixel (18.5×10^{-3} mm), and height equal to πD , which is Rayleigh's¹³ classical cutoff wavelength for the unstable perturbations of a constant flow, inviscid, jet of diameter D , when gravity is neglected. The graphed numbers correspond to the order in which the secondary satellite of the corresponding size pinched-off in a particular experiment.

Figure 6 shows that the size of the secondary satellites and the order in which they pinch-off are arbitrary. It appears that all but one observed secondary satellite drop has a size bigger than would result from a disturbance of the size of Rayleigh's¹³ cutoff wavelength. However, this secondary satellite was at the very limit of our resolution. We note that when the disturbances grow on the secondary thread, they create thinner regions in which pinch-off occurs. We cannot resolve the actual pinch-off within these thinner necks or smaller-scale satellite drops that may have formed.

One similarity in the details of the instability of the secondary thread, was that the instability occurred first in the leading half of the secondary thread in all experiments. This result is consistent with Brenner *et al.*'s⁹ prediction that the wave-like instability grows when $\xi < \xi^*$. A rough estimate of the wavelength of the disturbances in each experiment (assuming periodicity by counting the number of bulges in a given length) indicates that the wavelength varied by about a factor of 2 among experiments from about 0.4 to 0.8 mm. Figure 3(a-vii) shows an experiment in which the disturbance on the first-half of the secondary thread is fairly periodic, with a wavelength of about 0.7 mm. This range of wavelengths is an order of magnitude larger than the most unstable wavelength given by Rayleigh's¹³ calculation, which would be 0.08 mm. Kowalewski² observed that the wavelengths of instabilities on the secondary thread observed in jet breakup were orders of magnitude larger than Rayleigh's cutoff wavelength. We note that his secondary

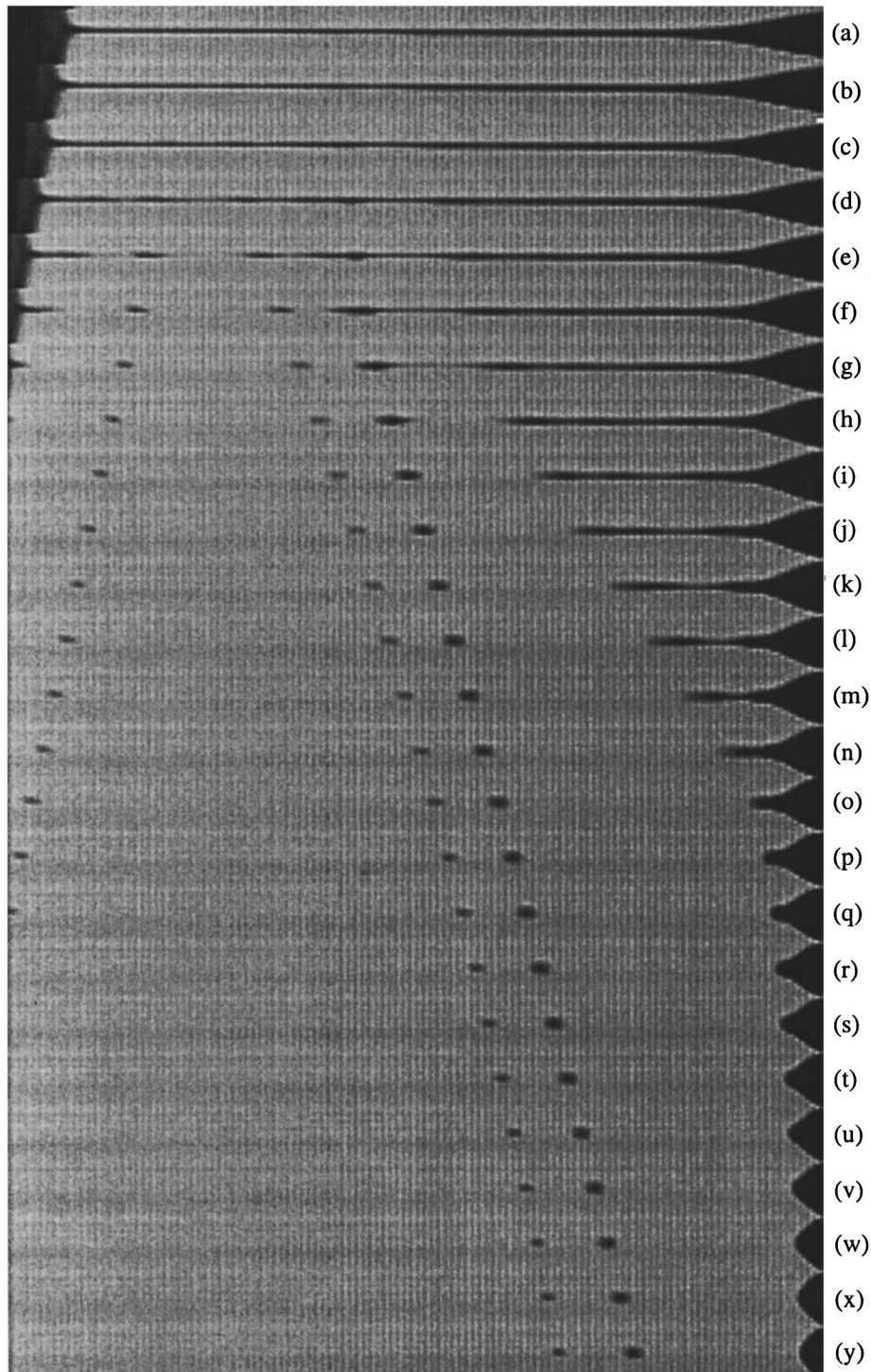


FIG. 5. Evolution of a secondary thread at the drop undergoing instability and multiple pinch-offs. The resolution is $18.5 \mu\text{m}/\text{pixel}$. The size of each image is $0.30 \times 4.40 \text{ mm}^2$. The time interval between successive images is $1/12\,000 \text{ s}$. $\nu = 96.0 \text{ mm}^2/\text{s}$.

threads, with widths of $1\text{--}3 \mu\text{m}$, were about an order of magnitude thinner than ours.

The breakup of the secondary thread does not look like the classic photographs of externally perturbed jet breakup examined by, e.g., Donnelly and Glaberson.¹⁴ In their experiments, a single photograph shows that the swollen part of the jet due to the growing wave grows in the downstream distance. Their measurements show that this growth is exponential with a constant rate well-predicted by Rayleigh's¹³ cal-

culations. In the present experiments, such a growth in the swollen parts of the unstable secondary thread is not observed in the downstream direction.

Figure 7 shows a more magnified [than Fig. 3(b)] view of the detachment of the thread from the remaining liquid at the orifice. (All of the images in Fig. 7 are from one experiment.) Here, the drop, which is not in view, is falling from right to left. The liquid remaining at the orifice is at the right-hand side of each image; the orifice itself, indicated by

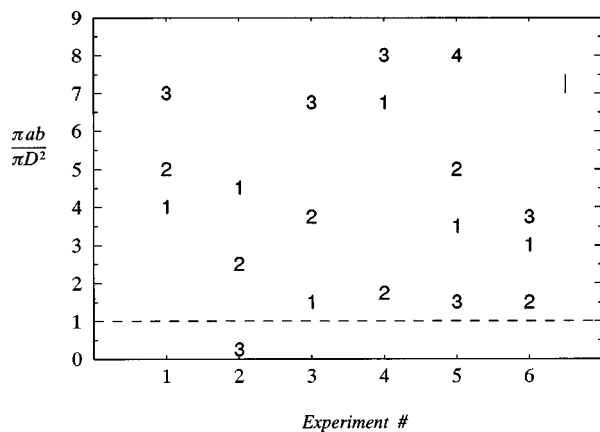


FIG. 6. Distribution of the size of the secondary satellite drops and their order of formation in six experiments. The dashed line estimates the size of a satellite drop that would have resulted from a Rayleigh mode with the cutoff wavelength. The vertical line at the upper right-hand side is the error bar. Viscosities are: experiment (1) 102.5 mm²/s; (2) 100.3 mm²/s; (3) 96.4 mm²/s; (4) 96.2 mm²/s; (5) 96.2 mm²/s; (6) 96.0 mm²/s.

the vertical line at the top right-hand side of Fig. 7, is 0.09 mm from the right-hand side of the image. Unlike the evolution of the primary to secondary thread that occurred at the drop, the primary thread at the orifice appears to neck down monotonically until its width is about the same as that of the secondary thread at the drop. (We note that observations further down the thread, out of the range of Fig. 7, do not show regions of curvature corresponding to a transition from primary to secondary thread.) Then, similar instabilities occur and pinch-off follows. Figures 7(a)–7(c) show the monotonic necking of the primary thread. Figures 7(d) and 7(e) show the formation of an instability. Figure 7(f) is the first image after pinch-off. The average distance between the two retreating tips in Fig. 7(f) is 1.23 mm from the orifice, showing that pinch-off does not occur at the point of maximum curvature near the orifice. A second pinch-off is observed in Fig. 7(g). The resulting secondary satellite is imparted with upward momentum so that it finally joins the liquid remaining at the orifice in the last image.

The most prominent difference between the pinch-off behavior of the primary thread from the drop and from the orifice is the formation of a distinct secondary thread in the first case and no such formation in the second. This result is in contrast to previous results reported by SBN¹ for a fluid with a comparable viscosity, a 100 cP glycerol and water mixture. In their experiment, both secondary and tertiary necks were observed at the orifice, just as were observed at the drop. The main difference between their experiment and ours was the size of the orifice, about 20 mm in diameter for SBN and 3.84 mm herein. Another difference is the values of surface tension of the two fluids. Theirs was probably about 66 g/s² (based on the measurement of 85% glycerol and water mixture reported by ZB¹⁰), while ours was 21.5 g/s².

The motion of the secondary satellite drops at the orifice is similar to the motion of their counterparts at the drop. That is, initially after the thread pinches off at the orifice, the shape of the secondary satellite drop changes significantly over a short time interval. An example is the secondary sat-

ellite drop closest to the orifice in Figs. 7(g)–7(i). During this period, the velocity of an arbitrary secondary satellite drop varies and may be either positive or negative. After its shape becomes essentially constant, its speed also is essentially constant. This behavior is seen for the same secondary satellite drop in figures 7(j)–7(s).

C. Speeds of the retreating threads

Figure 8 shows a comparison of measured speeds of the retreating secondary threads in three experiments with Eggers³ prediction, (1) with (2). The data displayed are for broken secondary threads that retreated to the primary thread; the behavior was qualitatively the same whether the retreat was to the drop or to the primary thread. In all of the experiments shown in Fig. 8, the measured speeds were obtained from the last of multiple pinch-offs along the secondary thread. The symbols represent the measurements; the solid curve is (1) with (2). In this comparison we chose $t_0 = 0$ to be the time halfway between consecutive frames before and after pinch-off.

The squares are from the pinch-off shown between Figs. 5(g) and 5(h). There is a bulge at the tip of the retreating thread due to the instability of the secondary thread. The speed of the retreating thread is fairly constant until this bulge joins the primary thread in about Fig. 5(n) for which $t' \sim 0.4$. Here, there is an abrupt drop in the velocity of the retreating thread's speed that is apparent in Fig. 8. The circles in Fig. 8 are from another experiment exhibiting similar behavior. This sudden drop in thread speed was common, since many of the retreating threads were characterized by a bulge due to the instability of the thread.

The diamonds represent an experiment in which pinch-off occurred so near the primary thread that the bulge retreated within one frame and the width of the retreating thread remained about constant during the remainder of the retreat; such experiments did not demonstrate the sudden drop in speed.

In general, the measured velocities are overpredicted by (1) with (2) by a factor of about 2 or 3 for $0.1 \leq t' \leq 0.4$ and by an order of magnitude for $t' \geq 0.4$. For $t' \leq 0.1$, the measurements and predictions do not agree; the predictions become infinite as $t' \rightarrow 0$, and we cannot resolve the speeds of the retreating threads as $t' \rightarrow 0$. Eggers²⁸ suggests that the predictions are larger than measurements because the theory does not take into account air drag on the retreating threads. The behavior shown in Fig. 8 for three experiments is representative of all our experiments.

Brenner *et al.*²⁹ measured the widths and distances of retreating threads from the pinch-off point as a function of time for high Reynolds-number flows. These quantities grew like $t'^{2/3}$, in agreement with the power law determined by Keller and Miksis,³⁰ who used scaling arguments for inviscid, surface-tension driven flows. The 2/3 exponent assumed that the shape of the recoiling tip was initially conical, which appeared to be true in the experiments. Brenner *et al.*²⁷ report, however, that numerical simulations, which resolved the threads closer to pinch-off than was possible in experiments, showed more complicated behavior. The shapes of the simulated tips were not simply conical, and exhibited a

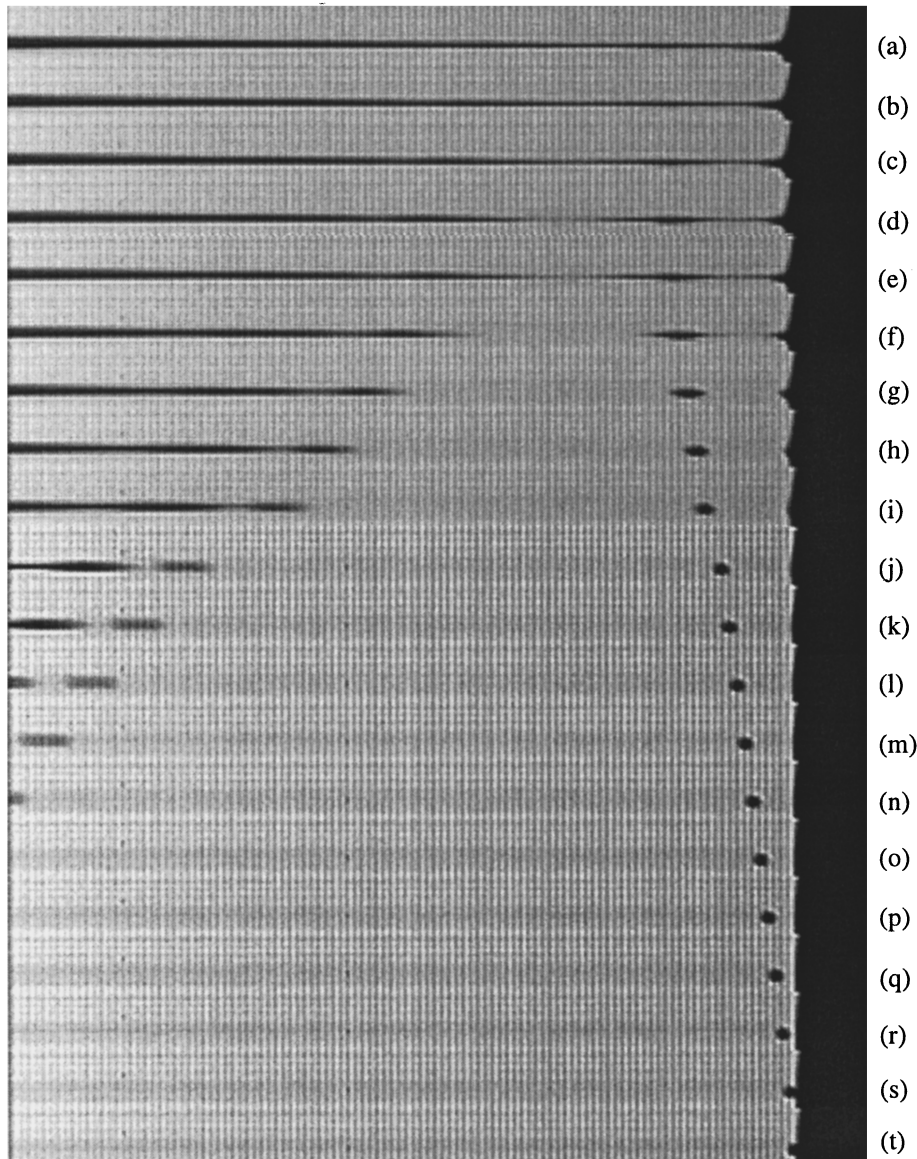


FIG. 7. Evolution of the primary thread during its pinch-off from the orifice. The resolution is $15.5 \mu\text{m}/\text{pixel}$. The size of each image is $0.25 \times 3.69 \text{ mm}^2$. The time interval between successive images is $1/12\,000 \text{ s}$. The line at the top, right-hand side shows the location of the orifice; $\nu = 100 \text{ mm}^2/\text{s}$.

‘crossover’ from one conical region to another of different size. They noted that in order for the time dependence of retreat to follow a power law, the initial shape of the retreating thread must follow a power law. If the distance of the thread from the pinch-off point follows a power law in time away from pinch-off, then the velocity of the retreating thread must also follow a power law.

To determine if the velocities, ν_{tip} , of the retreating threads herein had a power law dependence, i.e.,

$$\nu_{\text{tip}} = Ct'^{-a}, \quad (3)$$

we graphed the measured velocities on a log–log scale. Results are listed in Table II.

Experiment 1 in Table II corresponds to the diamonds in Fig. 8, in which the shape of the retreating thread remained fairly constant throughout the retreat. Threads in experiments

2–4 were characterized by a bulge that was present initially; a jump in velocity occurred when the bulge joined the primary thread. In experiments 2–4a the thread was retreating before the bulge joined the primary thread; in experiments 2–4b the thread was retreating after the bulge joined the primary thread. This behavior is shown in Fig. 5 (the squares in Fig. 8 and experiment 3 in Table II. The circles in Fig. 8 correspond to experiment 2.) The exponents for the retreating threads in experiments 2–4a are $\alpha < 1/2$, while those for experiments 2–4b are $\alpha > 1$. This marked difference is consistent with the notion that the speed of the retreating threads depends on its shape.

Experiments 5–7 are characterized by threads that broke a second time during their retreats. Results given for experiments 5–7a are from the first breaks in these experiments;

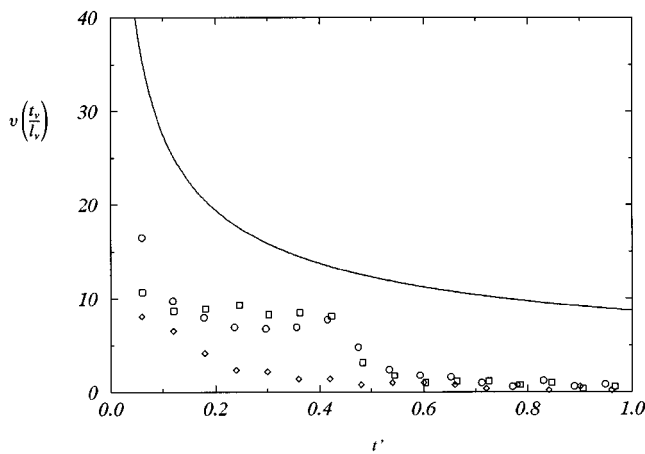


FIG. 8. Speeds of the retreating tips of the secondary threads after pinch-off for three representative experiments. Symbols: data (○) $\nu=96.6$ mm²/s; (□) $\nu=96.0$ mm²/s; (◇) $\nu=96.2$ mm²/s; (—) prediction using (1) with (2).

those given in experiments 5–7b are from the second breaks. Again, the first break has very low exponents, while the second break has exponents closer to, but less than, one.

To determine the power-law dependence, the time for pinch-off, t_0 , was used as a free parameter. It was varied until the data followed a line with a correlation coefficient listed in Table II. The starting point for estimating t_0 was the time halfway between the frame before and after pinch-off, in experiments 1, 2–4a, and 5–7a,b. Since we were unable to resolve the pinch-off time more closely, we varied t_0 by an amount (1/24 000 s) corresponding to the frames before and after pinch-off in these experiments. The values within these bounds that gave the highest correlation coefficients were chosen for the results depicted in Table II. In experiments

2–4b there were no bounds on the choices of t_0 because in these experiments there were no additional pinch-offs. The experiments depicted by squares and circles in Fig. 8 shows that in these type of experiments the velocities abruptly dropped when a bulge on the secondary thread joined the primary thread. Brenner *et al.*⁹ explained that a necking instability on the thread shifts the singular time. Here, the bulge on the retreating thread could play the role of the necking instability; thus, it is reasonable to assume that the threads in experiments 2–4b may also follow a power law, but referenced to a different singular time, t_0 .

In most experiments, the velocities did follow a power law. Figure 9 shows graphs of three experiments, the ones with the best and worst correlations to a line, and one with an exponent $\alpha > 1$. These results are also given in Table II.

Table II also shows images of the experiments in the first frame after pinch-off, or in the frame at which the velocity abruptly dropped due to a bulge joining the remaining fluid (experiments 2–4b). The images are presented to show the initial shapes of the retreating threads, which are required by the similarity laws. If the shapes of the retreating threads were initially parabolic, then the threads should have retreated with $\alpha=0.5$, in accordance with Eggers^{8,3} similarity solution. If the shapes were initially conical, they should have retreated with $\alpha=1/3$, in accordance with Keller and Miksis³⁰ similarity solution. The large variations in measured exponents, α , are consistent with the large variation in initial shapes as shown in Table II.

The inviscid scaling law given by Keller and Miksis³⁰ says that if the radius of the thread, $h \sim z^\beta$ while $v_{\text{tip}} \sim t'^{-\alpha}$, then $\beta=(2\alpha)/(1-\alpha)$. (This scaling law is also found in Brenner *et al.*²⁹) The values for β determined from the measured α listed in Table II for experiments 3–7a are

TABLE II. Correlation coefficients of a power-law fit of data to a line and measured constants and exponents corresponding to (3) for seven experiments exhibiting behavior described in the text. Experiments 1, 2a, and 7a correspond to data shown in Fig. 9.

Experiment#	Correlation Coefficient	C	α	Images of retreating threads after pinch-off
1	0.94	0.30	1.46	
2a	0.99	3.78	0.42	
2b	0.94	0.27	1.35	
3a	0.84	8.31	0.09	
3b	0.94	0.24	1.12	
4a	0.91	7.04	0.15	
4b	0.97	0.22	2.02	
5a	0.76	6.80	0.11	
5b	0.97	0.45	0.94	
6a	0.85	5.06	0.14	
6b	0.92	0.45	0.76	
7a	0.70	5.95	0.09	
7b	0.99	0.57	0.60	

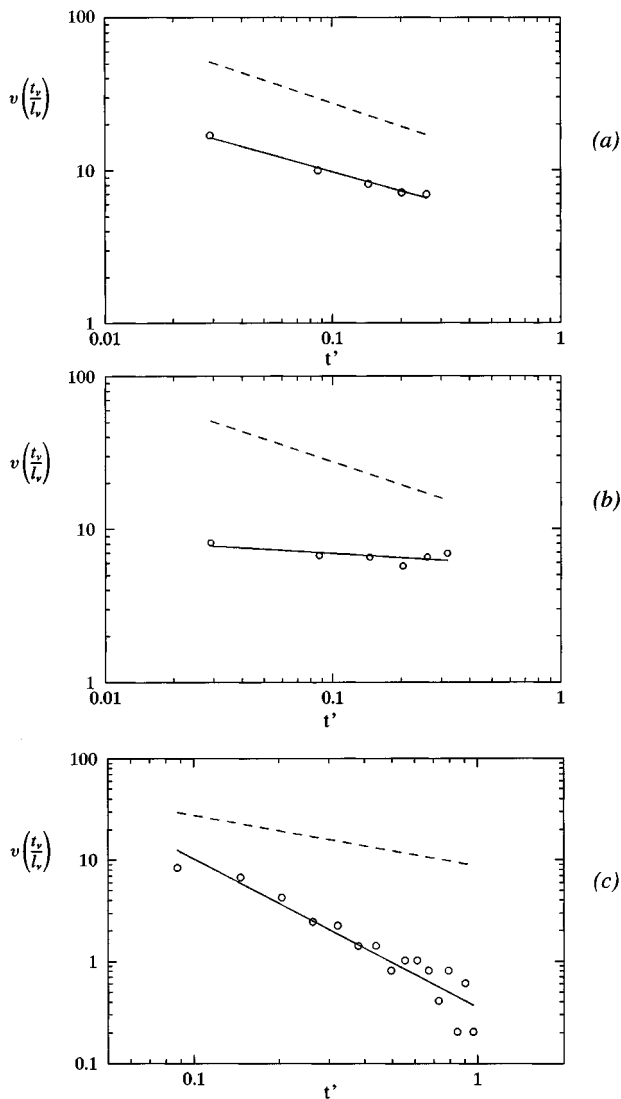


FIG. 9. Normalized velocities of retreating threads as a function of nondimensional time from pinch-off, $t' = (t - t_0)/t_v$. (○) Experimental data, (—) best fit to the data; (---) Eggers' predicted power law. (a) Experiment 2a in Table II; best correlation to a line. (b) Experiment 7a in Table II; worst correlation to a line. (c) Experiment 1 in Table II; $\alpha > 1$.

$0 < \beta < 1$. This result is roughly consistent with the long, thin, initial shapes of the retreating threads in these experiments as shown in the images in Table II. For experiments 5–7b, $\beta > 1$. This result is roughly consistent with the short, cuspy, initial shapes of the retreating threads in these experiments as shown in the images in Table II. For experiment 2a, $\beta = 1.45$. The initial shape of this retreating thread was long and thin, but it did have a pronounced bulge just behind its tip. The exponents measured for experiments 1, 2–4b are larger than one; therefore, the corresponding power law for the shape does not make sense. In particular, when $\alpha > 1$, $\beta < 0$, so h becomes unbounded as $z \rightarrow 0$. We note that the scaling law from Keller and Miksis³⁰ is for an inviscid fluid, while the fluid used herein is viscous.

IV. SUMMARY

Herein we have examined the pinch-off of viscous, pendant drops of fluid. A primary thread develops connecting

the drop to the orifice. It does not become unstable to a Rayleigh-type instability; instead, the primary thread becomes unstable to a secondary thread about 1/10 its width. This secondary thread does become unstable to a Rayleigh-type instability, resulting in pinch-off of the drop. For both the primary thread and the secondary thread, the slenderness ratio of width to length is about 0.005. It is not clear why the secondary thread and primary thread exhibit different types of instabilities. The pinch-off of the drop is not at the point of maximum curvature behind the drop—it is between the disturbances on the secondary thread. The instabilities on this secondary thread do not have a preferred wavelength. The wavelengths are an order of magnitude larger than the most unstable Rayleigh mode. Pinch-off at the orifice is different from pinch-off at the drop in that a distinct secondary thread does not form at the orifice. The speeds of the retreating tips follow a power law in time away from pinch-off. The power depends on the shape and the length of the retreating thread.

ACKNOWLEDGMENTS

We are grateful to Robert Geist, who built the experimental facility, and to Michael Brenner, Jens Eggers, Greg Forest, Steve Gharoff, Joe Hammack, Harvey Segur, and Simon Tavener for helpful discussions. The referees' comments helped substantially. Financial support for these experiments was provided by the National Science Foundation through Grant No. DMS92-57456, and by fellowships from the David & Lucile Packard Foundation and the Alfred P. Sloan Foundation. We are saddened by the death of our colleague, Bill Pritchard. We are honored to have collaborated with him on the problem of the "dripping tap."

- ¹X. D. Shi, M. P. Brenner, and S. R. Nagel, "A cascade of structure in a drop falling from a faucet," *Science* **265**, 219 (1994).
- ²T. A. Kowalewski, "On the separation of droplets from a liquid jet," *Fluid Dyn. Res.* **17**, 121 (1996).
- ³J. Eggers, "Theory of drop formation," *Phys. Fluids* **7**, 941 (1995).
- ⁴H. E. Edgerton, E. A. Hauser, and W. B. Tucker, "Studies in drop formation as revealed by the high-speed motion camera," *J. Phys. Chem.* **41**, 1029 (1937).
- ⁵D. H. Peregrine, G. Shoker, and A. Symon, "The bifurcation of liquid bridges," *J. Fluid Mech.* **212**, 25 (1990).
- ⁶R. M. S. M. Schulkes, "The evolution and bifurcation of a pendant drop," *J. Fluid Mech.* **278**, 83 (1994).
- ⁷J. Eggers and T. Dupont, "Drop formation in a one-dimensional approximation of the Navier–Stokes equation," *J. Fluid Mech.* **262**, 205 (1994).
- ⁸J. Eggers, "Universal pinching of 3D axisymmetric free-surface flow," *Phys. Rev. Lett.* **71**, 3458 (1993).
- ⁹M. P. Brenner, X. D. Shi, and S. R. Nagel, "Iterated instabilities during droplet fission," *Phys. Rev. Lett.* **73**, 3391 (1994).
- ¹⁰X. Zhang and O. A. Basaran, "An experimental study of dynamics of drop formation," *Phys. Fluids* **7**, 1184 (1995).
- ¹¹D. B. Bogoy, "Drop formation in a circular liquid jet," *Annu. Rev. Fluid Mech.* **11**, 207 (1979).
- ¹²S. E. Bechtel, C. D. Carlson, and M. G. Forest, "Recovery of the Rayleigh capillary instability from slender 1-D inviscid and viscous models," *Phys. Fluids* **7**, 2956 (1995).
- ¹³Lord Rayleigh, "On the instability of jets," *Proc. London Math. Soc.* **10**, 4 (1879).
- ¹⁴R. J. Donnelly and W. Glaberson, "Experiments on the capillary instability of a liquid jet," *Proc. R. Soc. London, Ser. A* **290**, 547 (1966).
- ¹⁵S. Chandrasekhar, *Hydrodynamic and Hydromagnetic Stability* (Dover,

- New York, 1970), a republication of the third printing (1970) of the original Clarendon Press edition (1961), pp. 523–542.
- ¹⁶E. F. Goedde and M. C. Yuen “Experiments on liquid jet instability,” *J. Fluid Mech.* **40**, 495 (1970).
- ¹⁷H. A. Stone, “Dynamics of drop deformation and breakup in viscous fluids,” *Annu. Rev. Fluid Mech.* **26**, 65 (1994).
- ¹⁸H. A. Stone, B. J. Bentley, and L. G. Leal, “An experimental study of transient effects in the breakup of viscous drops,” *J. Fluid Mech.* **173**, 131 (1986).
- ¹⁹H. A. Stone and L. G. Leal, “Relaxation and breakup of an initially extended drop in an otherwise quiescent fluid,” *J. Fluid Mech.* **198**, 399 (1989).
- ²⁰P. Lafrance, “Nonlinear breakup of a laminar liquid jet,” *Phys. Fluids* **18**, 428 (1975).
- ²¹N. N. Mansour and T. S. Lundgren, “Satellite formation in capillary jet breakup,” *Phys. Fluids A* **2**, 1141 (1990).
- ²²M. Tjahjadi, H. A. Stone, and J. M. Ottino, “Satellite and subsatellite formation in capillary breakup,” *J. Fluid Mech.* **243**, 297 (1992).
- ²³D. T. Papageorgiou, “On the breakup of viscous liquid threads,” *Phys. Fluids* **7**, 1529 (1995).
- ²⁴S. Kalliadasis and H.-C. Chang, “Drop formation during coating of vertical fibres,” *J. Fluid Mech.* **261**, 135 (1994).
- ²⁵S. A. Cryer and P. H. Steen, “Collapse of the soap-film bridge: Quasi-static description,” *J. Colloid Interface Sci.* **154**, 276 (1992).
- ²⁶R. M. S. M. Schulkes, “The contraction of liquid filaments,” *J. Fluid Mech.* **309**, 277 (1996).
- ²⁷E. A. Hauser, H. E. Edgerton, B. M. Holt, and J. T. Cox, Jr., “The application of the high-speed motion picture camera to research on the surface tension of liquids,” *J. Phys. Chem.* **40**, 973 (1936).
- ²⁸J. Eggers (private communication).
- ²⁹M. P. Brenner, J. Eggers, K. Joseph, S. R. Nagel, and X. D. Shi, “Breakdown of scaling in droplet fission at high Reynolds number,” submitted to *Phys. Fluids A*.
- ³⁰J. B. Keller and M. J. Miksis, “Surface tension driven flows,” *SIAM (Soc. Ind. Appl. Math.) J. Appl. Math.* **43**, 268 (1983).